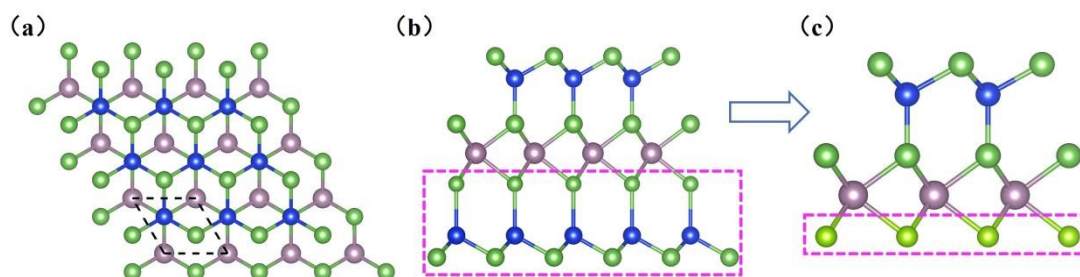


## Supplementary Information

### Spin Hall effect modulated by electric field in symmetric two-dimensional MoSiAs<sub>2</sub>Se



**Fig. S1.** (a) Top and (b) side views of the relaxed structure of MA<sub>2</sub>Z<sub>4</sub>. The purple, green, and blue balls represent the M, A, and Z atoms, respectively. The structure can be regarded as an MZ<sub>2</sub> triple layer [resembling 1H-phase MoS<sub>2</sub>; dashed rectangle in (b)] encapsulated by buckled AZ layers. (c) Diagram of the five-atomic-layer structure MoSiAs<sub>2</sub>Se, the pink dotted box is the evolution diagram.

Two-dimensional layered MoSi<sub>2</sub>N<sub>4</sub> and Wsi<sub>2</sub>N<sub>4</sub> were successfully prepared by chemical vapor deposition method. Since the IVB, VB, VIB, IVA and VA groups of many transition metal elements can replace their counterparts in MoSi<sub>2</sub>N<sub>4</sub>, these materials are extended to MA<sub>2</sub>Z<sub>4</sub> (M = Cr, Mo, W, V, Nb, Ta, Ti, Zr or Hf; A = Si or Ge; and Z = N, P, As), as shown in Fig. S1. We construct a five-atom-layer asymmetric MoSiAs<sub>2</sub>Se structure by removing A-Z atoms on one side and replacing the remaining A atoms on the same side with Se atoms. The single-layer MoSiAs<sub>2</sub>Se structure can be seen as the connection of the three-atomic layer of the MoS<sub>2</sub>-like Janus structure with the double-atomic layer of the sawtooth chain AZ structure. Fig. S1 is the construction diagram.

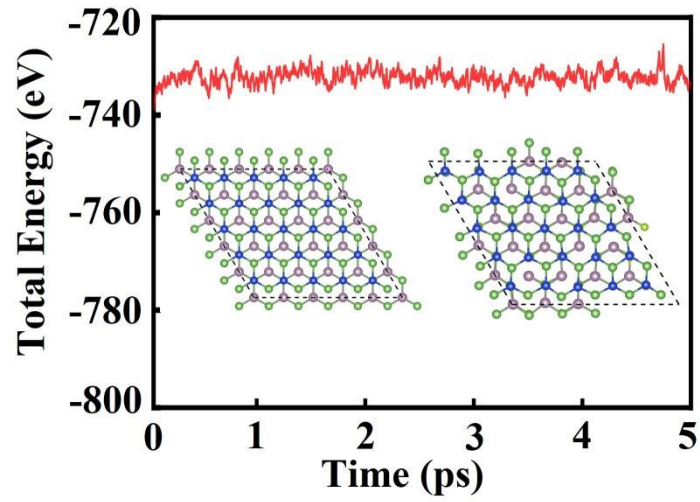


**Fig. S2.** Total energy of the structure  $\text{MoSiAs}_2\text{Se}$  as a function of simulation time at 300 K. The inset shows top and side views of the simulated structure.

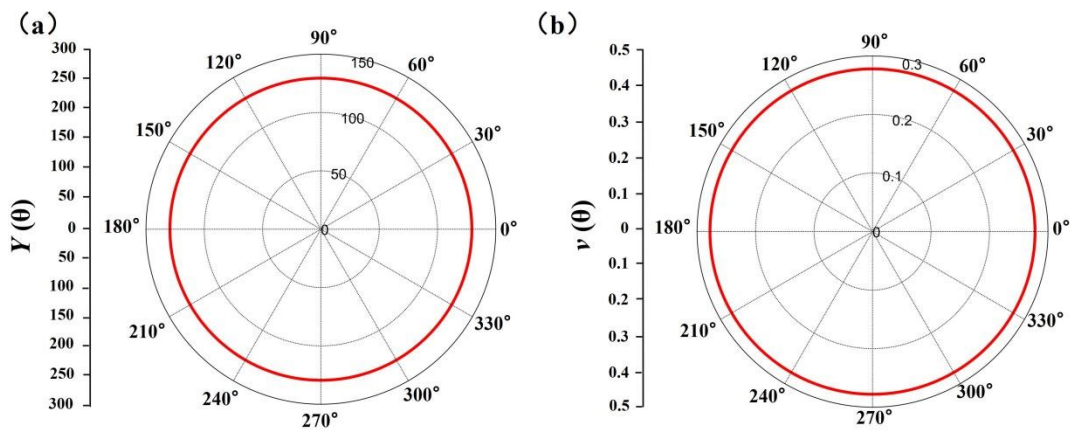


**Fig. S3.** The direction-dependent in-plane (a) Young's modulus and (b) Poisson ratio along an arbitrary direction  $\theta$ .  $\theta = 0^\circ$  corresponds to the x-axis.

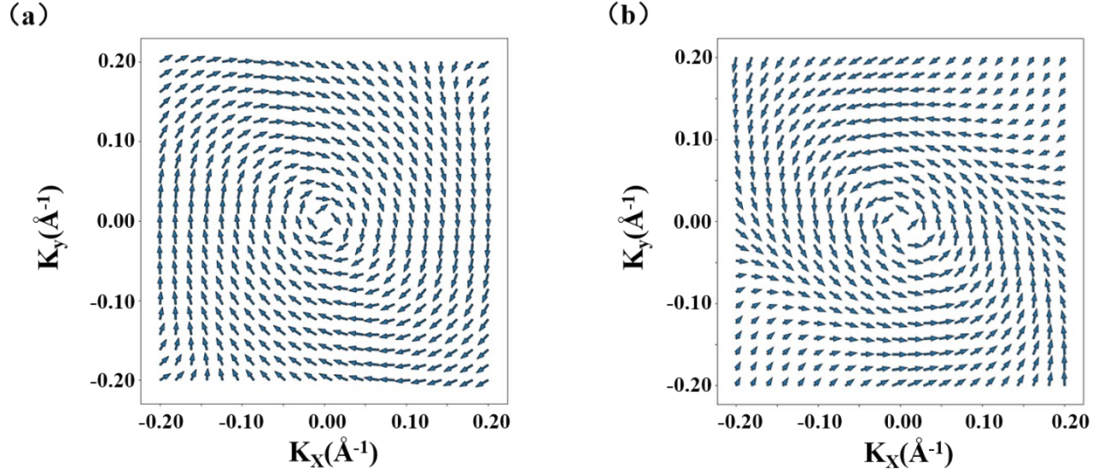


**Fig. S4.** (a) Spin textures of the red energy band of the Rashba spin-splitting near the  $\Gamma$  point. (b) Spin textures of the blue energy band of the Rashba spin-splitting near the  $\Gamma$  point.

To emphasize the Rashba-type spin splitting, we present the spin textures of the top two bands in the valence band around the  $\Gamma$  point in momentum space, as depicted in Fig. S4. An intriguing circular rotating texture is observed for the red and blue bands at the  $\Gamma$  point, wrapping around in opposite directions. The arrows indicate the in-plane component of the spin polarization. Furthermore, the nearly colorless background in the spin textures signifies the negligible presence of out-of-plane spin components. The distinct alignment of opposite spin directions in the internal and external branches and the presence of negligible out-of-plane spin components characterize the pure Rashba effect. Hence, the existence of Rashba-type spin splitting around the  $\Gamma$  point is firmly established.

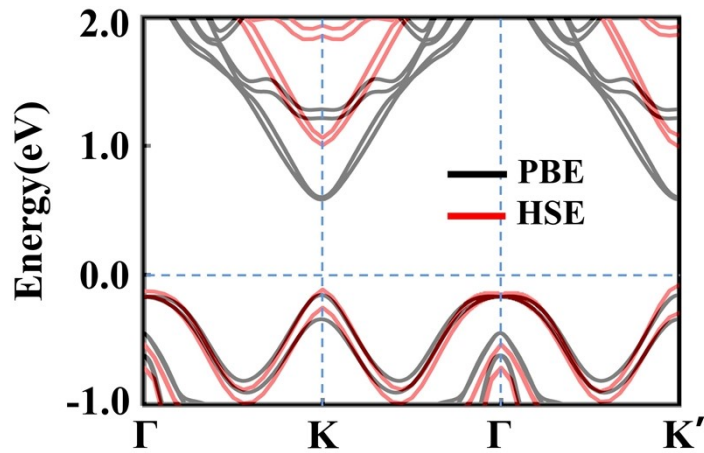


**Fig. S5.** Electronic band structure of monolayer MoSiAs<sub>2</sub>Se calculated with PBE (black lines) and HSE06 (red lines), respectively.

It was found that the band gap of HSE06 increased by 0.3212eV compared with the band gap of PBE functionalized. The Rashba parameter  $\alpha_R$  calculated by HSE06 is 0.604 eVÅ, and the valley splitting of VBM at K/K' is 139.8meV. By comparing the original Rashba parameter 0.597 eVÅ and the valley splitting parameter 187.3 meV, it is found that the difference in the band shape valley band and Rashba spin-splitting band near the band edge is negligible, which are more crucial for the spin transport properties.

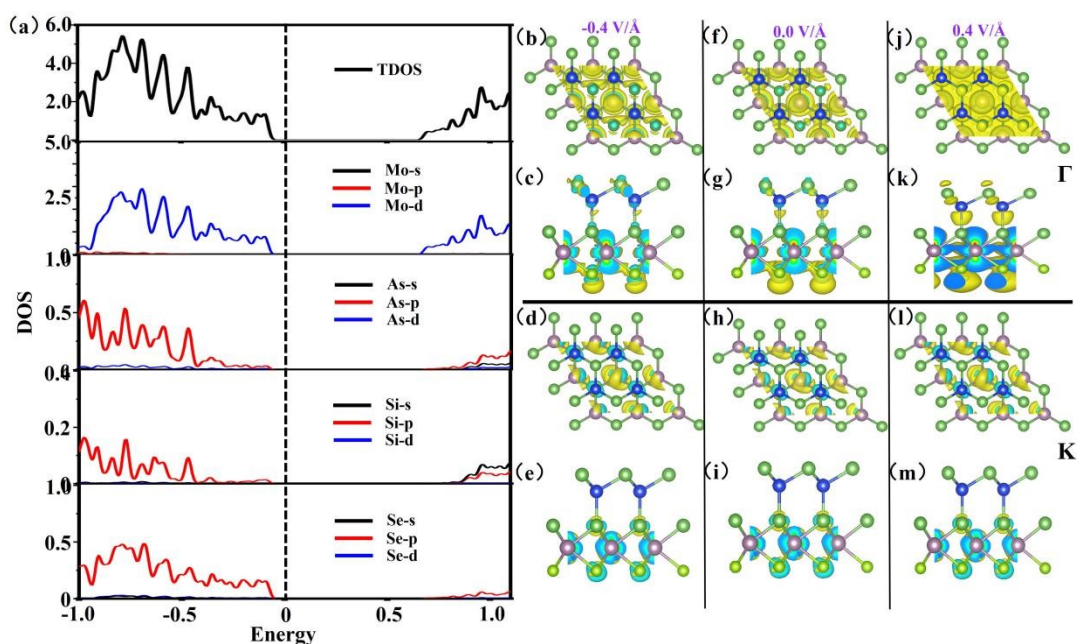


**Fig. S6.** (a) Density of States (DOS) and Projected Density of States (PDOS) for MoSiAs<sub>2</sub>Se monolayers under the influence of an external electric field. The Calculated band-decomposed charge density of valence bands near the Fermi level at the  $\Gamma$  and K points of

Janus MoSiAs<sub>2</sub>Se monolayers. The left panel, middle panel, and right panel showcase the partial charge density with decomposition for electric fields of  $-0.4 \text{ V/\AA}$ ,  $0 \text{ V/\AA}$ , and  $0.4 \text{ V/\AA}$ , respectively. The isosurface level is set to  $0.0003 \text{ bohr}^{-3}$ . The upper plane and lower plane denote the band-decomposed charge density of valence bands near the Fermi level at the  $\Gamma$  and K points, respectively. The letters b, f, j, d, h, l and c, g, k, e, i, and m represent the top view and side view of band decomposed charge density, respectively.

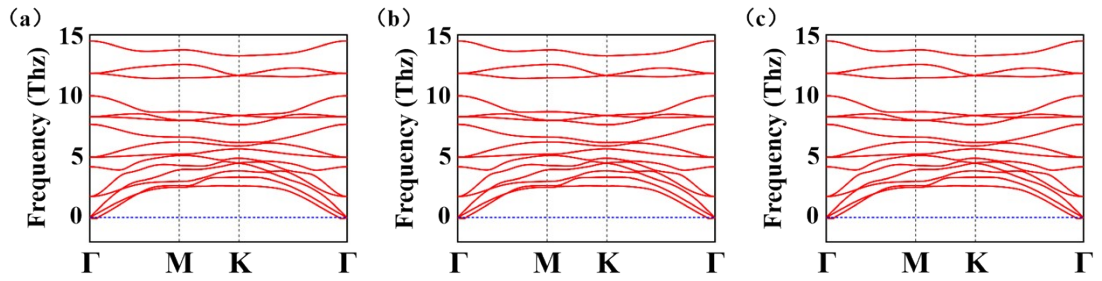


**Fig. S7.** (a)-(c) Phonon spectra of monolayer MoSiAs<sub>2</sub>Se at applied electric field  $-0.4 \text{ V/\AA}$ ,  $0.1 \text{ V/\AA}$  and  $0.4 \text{ V/\AA}$ , respectively.

**Fig. S7.** shows the phonon spectrum for  $-0.4, 0, 0.4 \text{ V/\AA}$ . We find no imaginary frequencies appear in the whole Brillouin zone (BZ), confirming their dynamical stability.

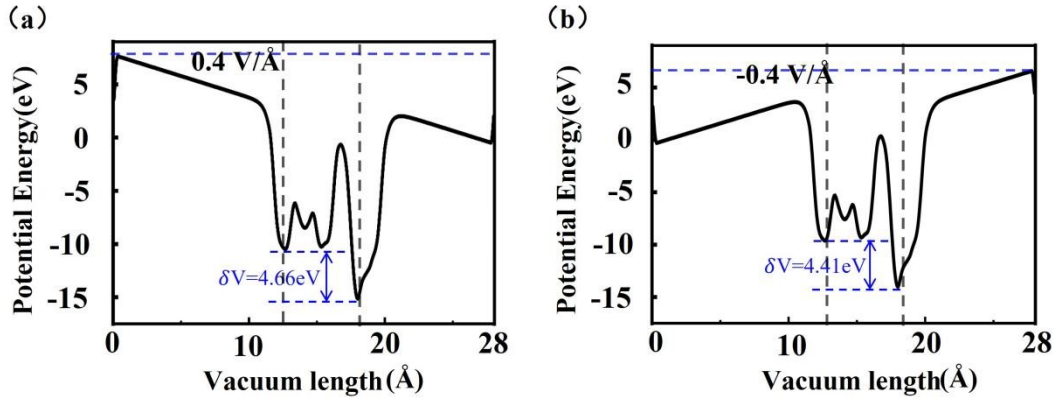


**Fig. S8.** Potential drop across the MoSiAs<sub>2</sub>Se heterostructure with (a) Electric field = 0.4 V/Å, (b) Electric field = -0.4 V/Å.

The in-built potential in the MoSiAs<sub>2</sub>Se is also affected by the external electric field, as shown in Fig. S8. The potential drop or the inbuilt electrostatic field is enhanced by applying a positive electric field and is reduced by applying a negative electric field.

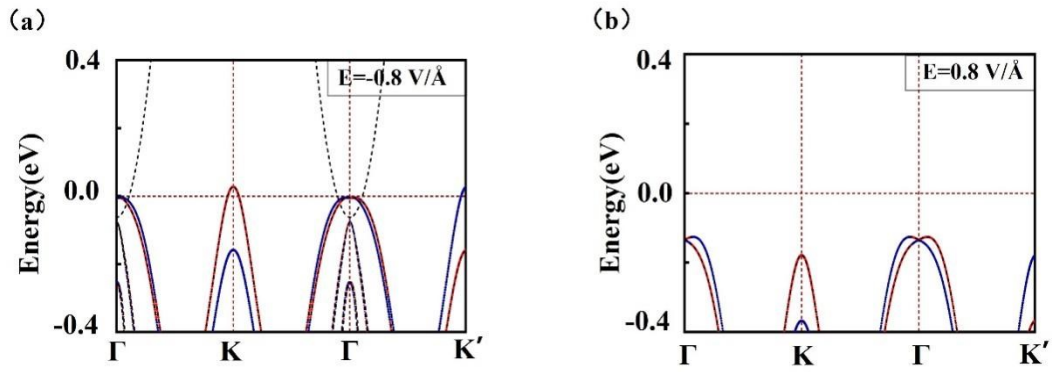


**Fig. S9.** (a-b) in the figure represent the applied electric field MoSiAs<sub>2</sub>Se energy band diagrams for -0.8 and 0.8V/Å, respectively.

## Reference

1. J. Yuan, Q. Wei, M. Sun, X. Yan, Y. Cai, L. Shen and U. Schwingenschlögl, *Physical Review B*, 2022, **105**, 195151.
2. Q.-F. Yao, J. Cai, W.-Y. Tong, S.-J. Gong, J.-Q. Wang, X. Wan, C.-G. Duan and J. H. Chu, *Physical Review B*, 2017, 95.
3. F. Mouhat, F. X. Coudert, *Physical Review B*, 2014, **90**, 224104.